Freeze casting of LAGP for 3D textured solid-state structural electrolytes

Will Huddleston[1], Frederick Dynys[2], Alp Sehirlioglu[1]

[1]Case Western Reserve University, Dept. Materials Science and Engineering, Cleveland, OH 44106, USA

[2]NASA Glenn Research Center, Cleveland, OH 44135, USA

Objective:

- Characterize processing-structure-property relationships governing freeze casting of $Li_{1.5}Al_{0.5}Ge_{1.5}(PO_4)_3$ NaSICON solid electrolyte.
- Evaluate production of thin solid-state electrolyte separators with high porosity and interfacial area for improved active material loading.

Motivation:

- Enable next generation **hybrid-electric** and **all-electric** aerospace propulsion systems for green aviation, seek to reduce emissions and achieve higher efficiency.
- Novel solutions are needed to increase **energy density** and achieve systems level **weight savings** in inherently **safe** configurations.

Figure 1: Leading Edge Asynchronous Propeller Tech.

https://www.nasa.gov/centers/armstrong/features/leaptech.html

Background

All-solid-state batteries

- Prevent Li dendrite growth, improve safety.
- Reduce parasitic inactive components, improve Ah/g.

Multifunctional Energy Storage

- Figure of Merit – systems level weight savings.
- Active battery materials in load bearing paths.

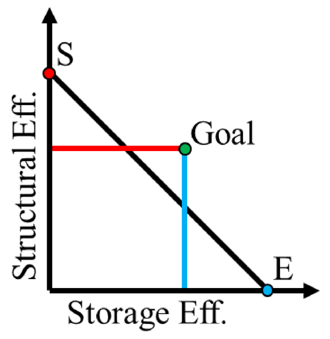

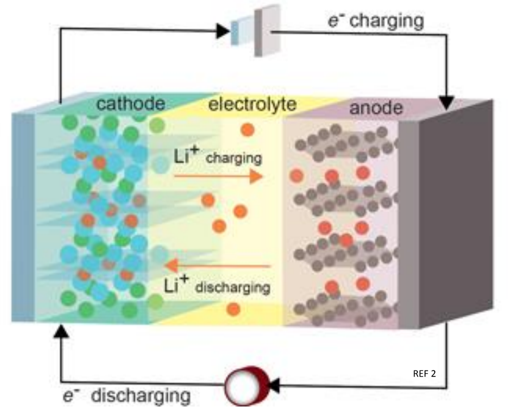

Figure 2: Lithium-ion battery schematic.

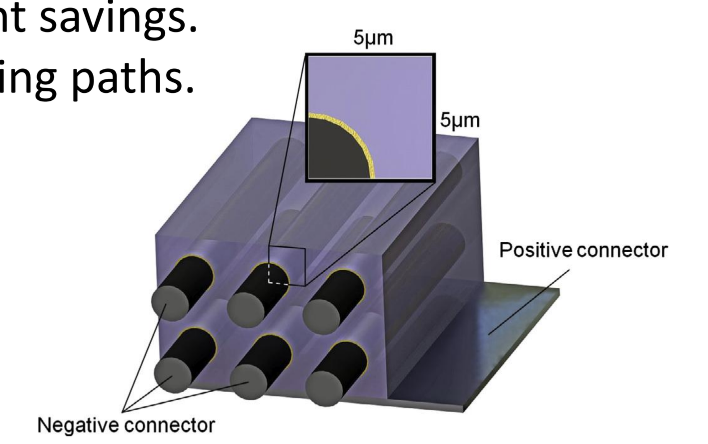

Figure 3: State of the art structural battery: carbon fiber anode, polymer electrolyte coating, cathode containing matrix

"Ion exchange in a lithium ion battery" PANalytical X'Press 3/2015 URL: http://www.panalytical.com/Press-room/XPress-magazine/XPress-32015-4.htm Accessed 4/2/17. Ekstedt, S., Wysocki, M., Asp, L.E., 2010. "Structural batteries made from fibre reinforced composites." Plastics, rubber and composites 39, 148–150

Freeze Casting Overview

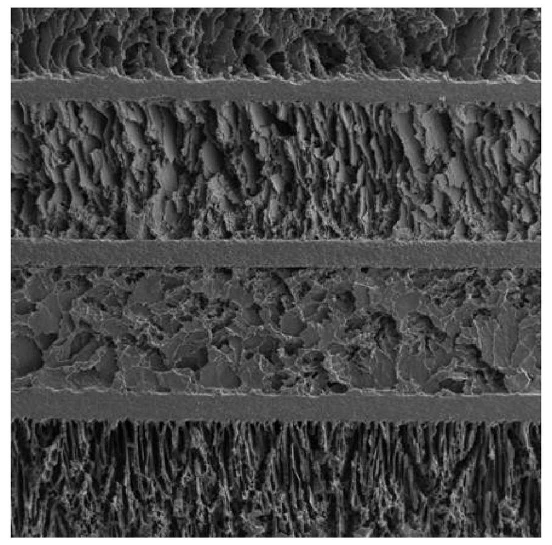

Figure 4: Inspiration from freeze cast functional ceramics implemented as SOFC electrodes, developed at NASA GRC.

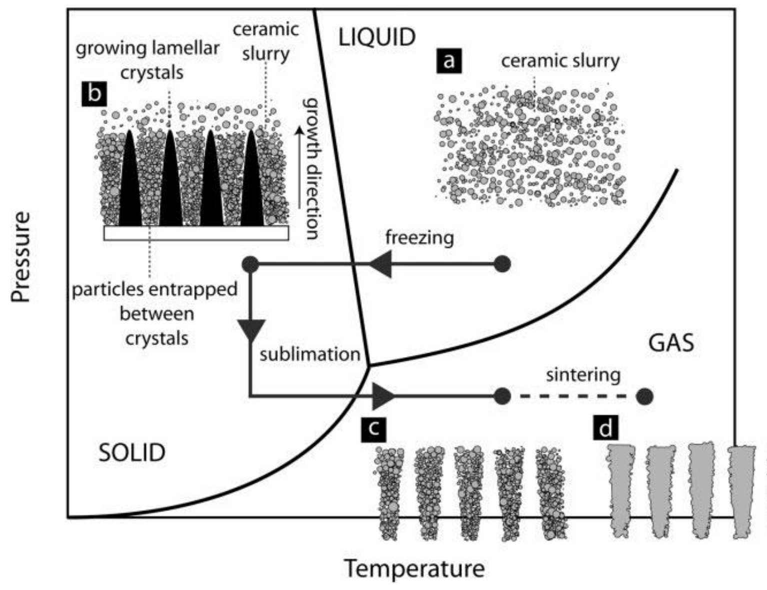

Figure 8: Four processing steps:
1) Aqueous slurry preparation
2) Freeze tape casting
3) Sublimation
4) Burnout and Sintering

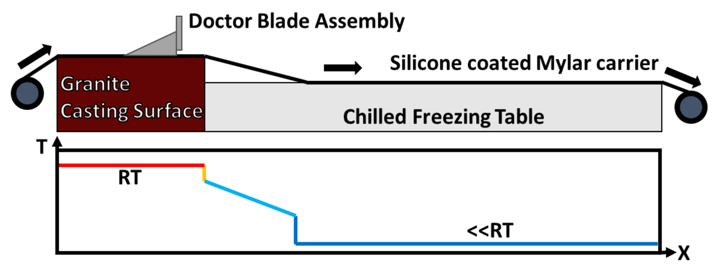

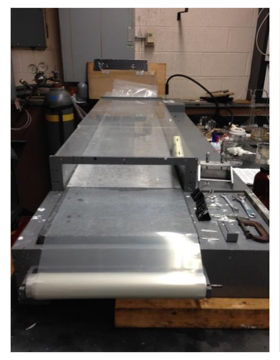

Figure 5: Casting table and temperature profile.
Figure 6: Freeze casting table displaying mylar carrier and granite casting surface.
Figure 7: Freeze dryer for sublimation of ice from green tapes.

T.L. Cable, J.A. Setlock, S.C. Farmer, A.J. Eckel: "Regenerative performance of the NASA symmetrical solid oxide fuel cell design", Int. J. Appl. Ceram. Technol., 8 [1] 1–12 (2011)
S. Deville, "Freeze-Casting of Porous Ceramics: A Review of Current Achievements and Issues" ADVANCED ENGINEERING MATERIALS 2008, 10, No. 3

Ice Templating Kinetics

	Component	Composition
Constants	Solids	LAGP
	Dispersant	Darvan C-N
	Surfactant	Dynol 604
	Binder	B-1000/B-1022
		Methyl Cellulose
		Polypropylene Carbonate
Variables	Plasticizer	PEG
		Glycerin
	Solvent	H2O
		H2O + EthOH
		H2O + IPA
	Thickener	XG

Casting Variables
Carrier Velocity
Carrier Composition
Table Temperature
Slurry Temperature
Freezing Temperature
Doctor Blade Height
Casting Angle

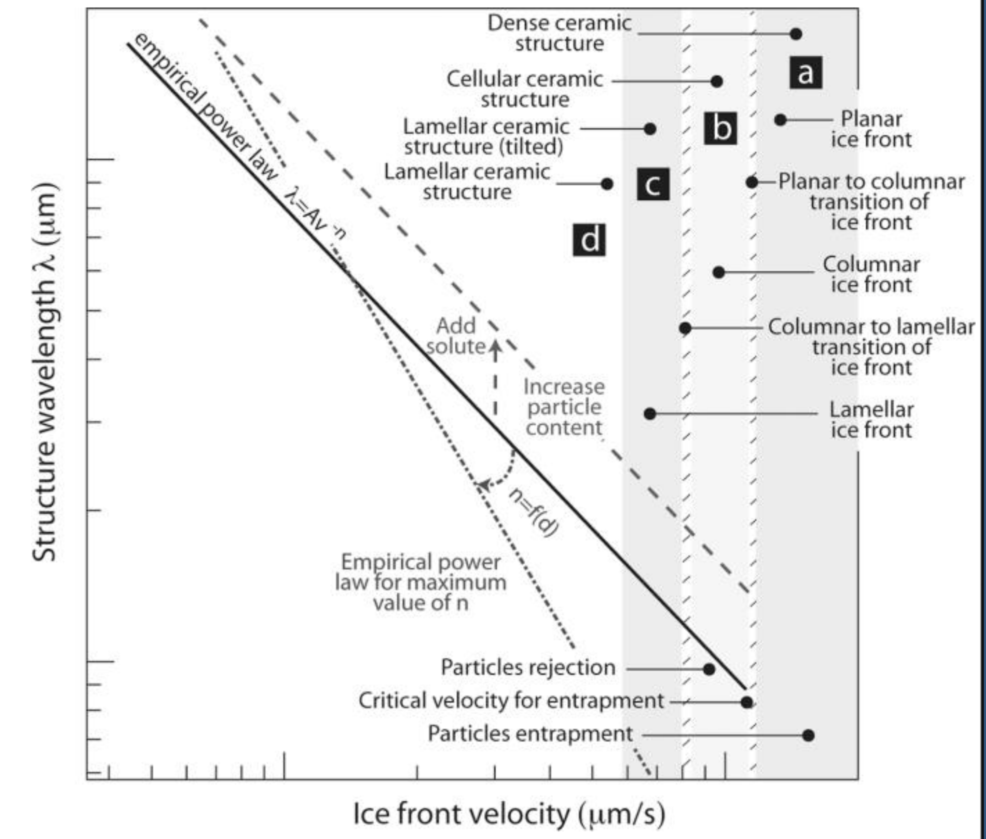

Figure 9: Kinetic zones for desired microstructures.

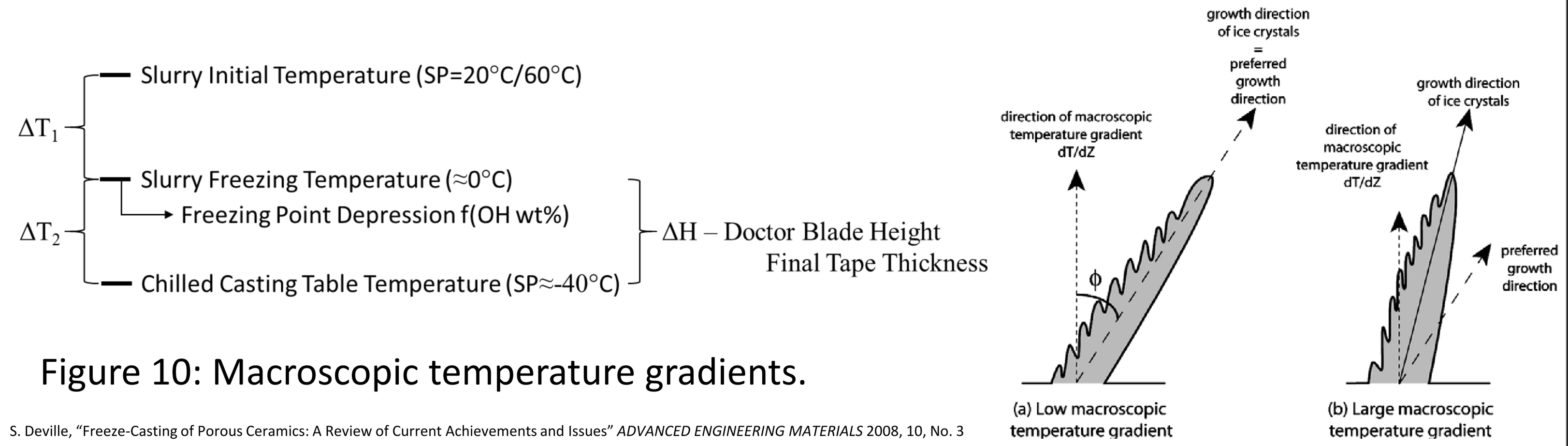

Figure 10: Macroscopic temperature gradients.

S. Deville, "Freeze-Casting of Porous Ceramics: A Review of Current Achievements and Issues" ADVANCED ENGINEERING MATERIALS 2008, 10, No. 3

Microstructural Control

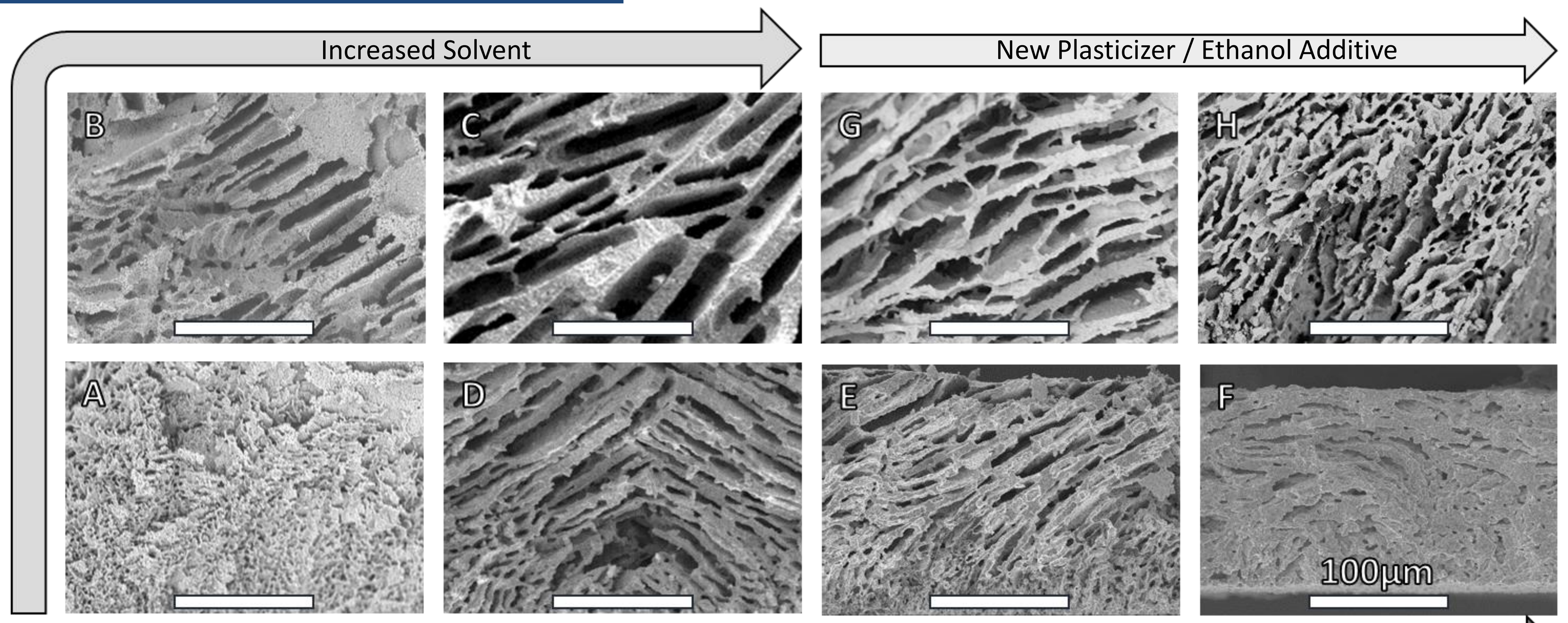

Solids	Dispersant	Surfactant	T-Slurry
25g LAGP	0.5g Darvan C	0.15g Dynol 604	20C

Slurry Preperation					Casting Parameters		
ID	Solvent	Xantham Gum Thickener	Methyl cellulose Binder (10wt% loading)	Plasticizer	T-Table (°C)	Blade Height (in)	Casting Speed
A	15g H2O	0.1wt%	10g	N/A	-25	0.06	40%
B	28.8g H2O			3wt% PAG	-25	0.08	
C	26.5g H2O			6wt% PAG	-15	0.2	
D	33g H2O		11g	6.6wt% PAG	-25	0.06	
E	33g H2O			10wt% PAG	-25	0.04	
F	33g H2O			15wt% PAG	-25	0.03	
G	52g H2O			10wt% PAG + 10wt% PEG	-10	0.08	
H	40mL H2O / 5mL EthOH (10wt%)	1wt%		5wt% PEG	-20	0.08	25%

Figure 11: Freeze cast LAGP microstructures, slurry compositions, and casting parameters.

- ABC: Increased solvent volume, resulted in increase in templated porosity.
- DEF: Increased plasticizer (PAG) content due to cracking of tapes during sublimation. Resulted in decreased porosity. High plasticizer content stabilized transformation front.
- GH: Changed plasticizer (PEG), resolved residual cracking. Templated porosity recovered, ethanol ΔT modified.
- Changes in slurry composition yielded significant changes to microstructural characteristics.
- Porosity and vertical directionality increased.

Thermal Imaging

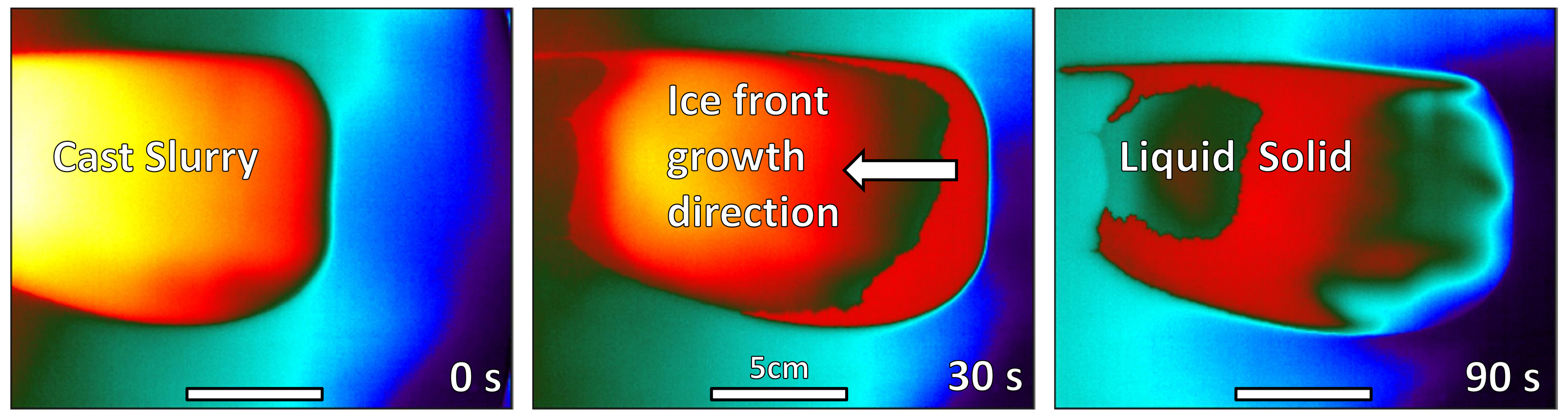

Figure 12: Top down view of infrared thermal imaging.

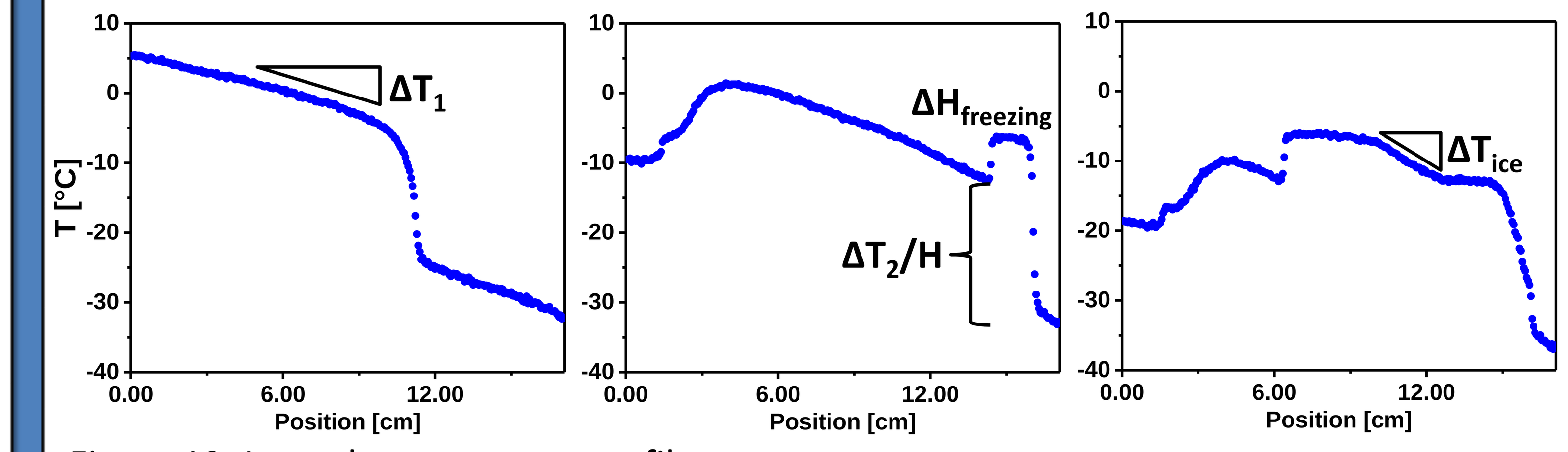

Figure 13: Lateral temperature profiles.

Infrared imaging enabled direct observation of thermal environment.

- ΔT_1 lateral thermal gradient
- ΔT_2 vertical thermal gradient
- ΔH exothermic solidification
- ΔT_{ice} heat removal after transformation
- Nucleation versus growth preference

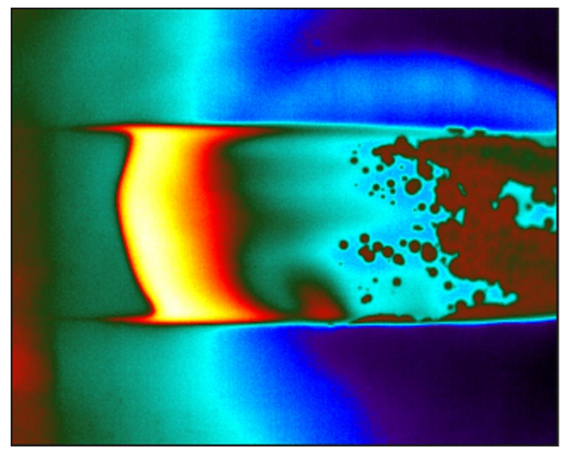

Figure 14: Undesirable nucleation preference.

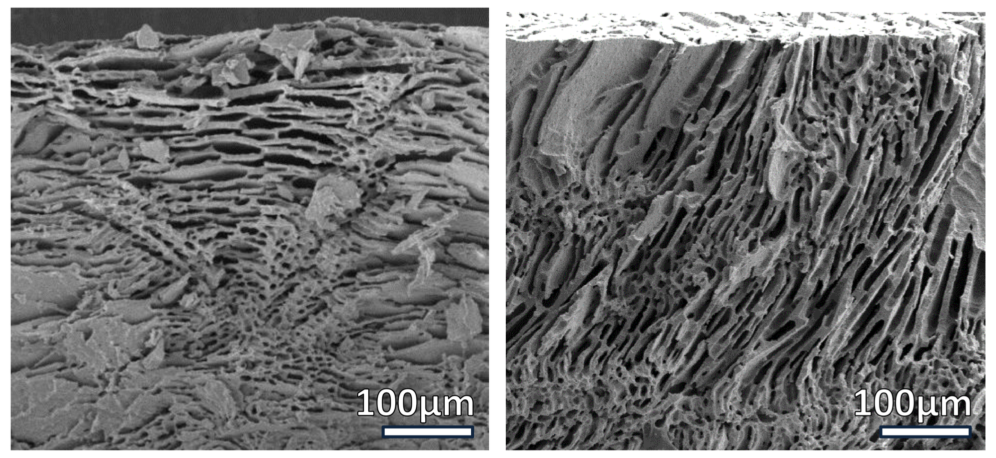

Figure 15: Observed improvements to directionality by preheating slurry.

Future Work

- Multifunctional performance characterization
  - Electrochemical impedance spectroscopy
  - Ring-on-ring biaxial flexure fracture testing
  - Cycling performance

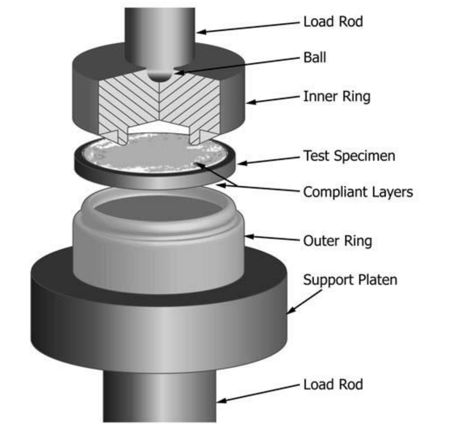

Conclusions:

- Slurry composition and casting parameters were tuned to provide desirable microstructural traits: high porosity and vertical directionality.
- Relationships between macroscopic experimental observations and local microstructural properties were explored.
- Direct observation of macroscopic thermal environment was achieved through infrared imaging.

Acknowledgements: Tom Sabo, Ray Babudar, John Setlock